Journal of Power Sources 195 (2010) 8152–8161

Contents lists available at ScienceDirect

Journal of Power Sources

journal homepage: www.elsevier.com/locate/jpowsour

Flame spray deposition of $La_{0.6}Sr_{0.4}CoO_{3-\delta}$ thin films: Microstructural characterization, electrochemical performance and degradation

Nikolaos. I. Karageorgakis[a,*], Andre Heel[a], Anja Bieberle-Hütter[b], Jennifer L.M. Rupp[b], Thomas Graule[a], Ludwig J. Gauckler[b]

[a] Laboratory for High Performance Ceramics, EMPA, Swiss Federal Laboratories for Materials Testing and Research, Ueberlandstrasse 129, CH-8600 Dübendorf, Switzerland
[b] Institute of Nonmetallic Inorganic Materials, Department of Materials, ETH Zürich, Wolfgang-Pauli Str. 10, CH-8093 Zürich, Switzerland

ARTICLE INFO

Article history:
Received 18 April 2010
Received in revised form 16 June 2010
Accepted 24 June 2010
Available online 1 July 2010

Keywords:
Thin films
Flame spray deposition
Electrochemistry
Microstructure
Cathode

ABSTRACT

Thin films of $La_{0.6}Sr_{0.4}CoO_{3-\delta}$ (LSC) were deposited by flame spray deposition at a deposition temperature of 200 °C. The as-deposited LSC films were dense, particle-free and amorphous. Upon annealing above 600 °C, the films crystallized into the rhombohedral perovskite LSC phase. For isothermal annealing at higher temperatures parabolic grain growth kinetics occur in parallel to densification of the thin films. Electrochemical measurements on symmetrical cells with LSC films on CGO pellets showed lowest area specific resistance (ASR) of 0.96 Ω cm^2 at 600 °C for films of 38 nm in grain size annealed at 700 °C. Degradation of the ASR of the LSC films of 3.9% was found after 5 days operation at 550 °C in ambient air.

1. Introduction

Solid Oxide Fuel Cells (SOFCs) operate typically in the temperature regime of 800–1000 °C to ensure a sufficiently high power output [1,2]. A state-of-the-art cathode material used in conventional SOFCs is the perovskite $La_{1-x}Sr_xMnO_{3-\delta}$ (LSM), deposited on an yttria-stabilized zirconia (YSZ) electrolyte [3]. In the overall SOFC power output, highest losses result from the nonlinear overpotential at the cathode–electrolyte interface [4]. Particularly for the YSZ/LSM system, the reduced performance is assigned mainly to the surface-dominated oxygen transfer kinetics of the purely electronic conducting LSM cathode [5]. Therefore, alternative materials with mixed ionic-electronic conductivity (MIEC) have been investigated, such as $La_{1-x}Sr_xCoO_{3-\delta}$ (LSC) [6,7], $La_{1-x}Sr_xFe_{1-x}Co_xO_{3-\delta}$ (LSCF) [8,9], $Ba_{1-x}Sr_xFe_{1-x}Co_xO_{3-\delta}$ (BSCF) [8,10–15], and $Ba_{1-x}Sr_xFe_{1-x}Zn_xO_{3-\delta}$ [14,16]. Due to the mixed conductivity, volume diffusion occurs in addition to surface diffusion and accelerates the oxygen transfer kinetics of these MIEC perovskites compared to LSM [5]. Among these perovskites the lanthanum strontium cobaltite reveals a higher structural stability compared to BSCF, which decomposes for residual CO_2 contamination from the air during cathode operation [8,10,12]. However, the weakness of the lanthanum-based cathodes relies in its tendency to form insulating $La_2Zr_2O_7$ phases at the standard La-cathode/YSZ interface [17–19] and the large mismatch in the thermal expansion coefficient ($TEC_{LSC} = 19.6 \times 10^{-6}\,K^{-1}$) [20] with the YSZ ($TEC_{YSZ} = 10.9 \times 10^{-6}\,K^{-1}$) [21] leading to a drop in the power output. Alternative electrolytes or interfacial buffer layer based on ceria may be used to solve the problem of reactivity between cathode and electrolyte [22,23], but still the large TEC mismatch with the LSC results in high degradation during the operation of the SOFCs. A viable solution to the TEC mismatch and existence of lanthan-zirconate formation [6,24] that has also a beneficial influence on the whole operation of the SOFCs, is the reduction of the operating temperature below 600 °C [25,26]. A special type of a SOFC operating at low to intermediate temperatures is the micro-SOFC for the application of battery replacement in portable electronic devices [27,28]. For these micro-SOFCs, cathodes processed as thin films [29] are an absolute requirement since the active fuel cell forms a free-standing membrane of less than 1 μm in thickness, integrated on a wafer substrate, e.g., Si [30–33] or Foturan glass–ceramic wafer [34,35]. Latter substrates do not withstand higher temperatures than 800 °C without damage and thus limit the fuel cell operation temperature regime. Recently, first power performance data of micro-SOFCs with LSCF thin films by sputtering [36] and spray pyrolysis [34] were published. These show promising power characteristics compared to conventional Pt-based metal film cathodes of micro-SOFCs exhibiting strong microstructural degradation during operation. In literature promising cathode thin

* Corresponding author. Tel.: +41 765 486 390.
E-mail addresses: nikarageo@gmail.com, nkarageo@student.ethz.ch (Nikolaos.I. Karageorgakis).

0378-7753/$ – see front matter © 2010 Elsevier B.V. All rights reserved.
doi:10.1016/j.jpowsour.2010.06.089

films were reported for potential micro-SOFCs. More specifically, LSC thin films were deposited by vacuum-based techniques, such as pulsed laser deposition (PLD) [6,37–41], radio frequency sputtering [42], laser ablation [43–45] and precipitation-based ones, such as metalorganic deposition (MOD) [24,46], sol–gel [47,48], ultrasonic spray pyrolysis [49] and electrostatic spray assisted vapour deposition (ESAVD) [50].

We have recently reported for the first time the application of flame spray deposition technique, a novel precipitation-based thin film preparation process, to deposit high-quality $Ce_{0.8}Gd_{0.2}O_{1.9-\delta}$ electrolyte thin films of 450 nm film thickness [22]. In latter reference the deposition mechanism has been investigated in detail. The advantages of this method include the very high deposition rates of about 30 nm min^{-1} compared to other thin film processes, which are limited to a few nm min^{-1} and the low deposition temperatures of 200 °C. Furthermore, no vacuum is required for the deposition, it is easy to scale-up and it is possible to coat large areas with low processing cost [8].

For this work, the flame spray method has been used to deposit dense and particle-free LSC films. The microstructural characteristics of the flame-deposited LSC films have been investigated and correlated with the ASR of half-cells based on ceria electrolytes. The degradation of the LSC films over 120 h was studied to evaluate their potential as cathodes for micro-SOFC membranes.

2. Experimental

Thin films of $La_{0.6}Sr_{0.4}CoO_{3-\delta}$ (LSC) have been deposited by flame spray deposition. In this technique, a liquid solution is prepared by mixing suitable precursors and is fed by a syringe pump into the flame. The precursor solution is atomized through a centre capillary, surrounded by the outlet for the dispersion gas, which atomizes then the precursor into the flame. The experimental setup has been described in detail elsewhere [22]. The flame is created by igniting a mixture of 2 l min^{-1} CH_4 and 7 l min^{-1} O_2. The flow of the dispersion O_2 is 20 l min^{-1} for all experiments and the flow rate of the precursor solution is 0.5 ml min^{-1}. The precursor solution consisted of lanthanum nitrate ($La(NO_3)_3{\cdot}6H_2O$, Sigma–Aldrich, 99% purity), strontium chloride ($SrCl_2{\cdot}6H_2O$, Sigma–Aldrich, 99% purity) and cobalt nitrate ($Co(NO_3)_2{\cdot}6H_2O$, Sigma–Aldrich, 98% purity), dissolved in N,N-dimethylformamide (DMF, Fluka, 98% purity) to form a solution of 0.006 M. The LSC thin films have been deposited on sapphire substrates (Stettler, Switzerland) for microstructural investigation and on $Ce_{0.9}Gd_{0.1}O_{2-\delta}$ pellets for electrochemical characterization. The deposition temperature (200 °C) has been monitored by positioning a thermocouple (accuracy ±10%) at the back of the substrates.

The morphology of the thin films was characterized by scanning electron microscopy (SEM, Leo 1530, Germany) with an attached energy dispersive X-ray detector. Grain sizes in the LSC films were determined by measuring more than 300 grain intercept lengths of three different spots on the films, using a conversion factor of 1.56 in the Lince software [51]. Porosity was evaluated by using the Gatan DigitalMicrograph microscopy software. X-ray diffraction (XRD, Siemens S5000, Germany) was performed using Bragg–Brentano configuration from 20° to 80° with step size of 0.05° and scan time of 8 s $step^{-1}$. The crystallographic density was calculated by fitting the XRD spectra with HighScore Expert software and using the Dicvol calculation method.

For the electrochemical characterization, the LSC films were deposited for 10 min symmetrically on CGO pellets using a shadow mask with dimensions of 1 cm × 1 cm. The symmetrical cells were heat treated for 10 h at the final annealing temperature of the LSC films, in order to crystallize the initially amorphous as-deposited films. These heat treatment conditions were chosen based on the crystallization of $Ce_{0.8}Gd_{0.2}O_{1.9-\delta}$ (CGO) thin films prepared by the same method in our previous work [22]. The CGO pellets were prepared by pressing uniaxially with a pressing force of 40 kN, 4 g of $Ce_{0.9}Gd_{0.1}O_{2-\delta}$ powder (Starck GmBH, Germany), followed by high temperature sintering for 2 h at 1650 °C at 5 °C min^{-1}. More details of the sintering can be found in Ref. [8]. Prior to thin film deposition, the CGO pellets were grinded and polished for 20 min on Si paper. On top of the LSC films, approximately 5 μm of Pt paste (Heraeus C 3605 P) was painted using a brush.

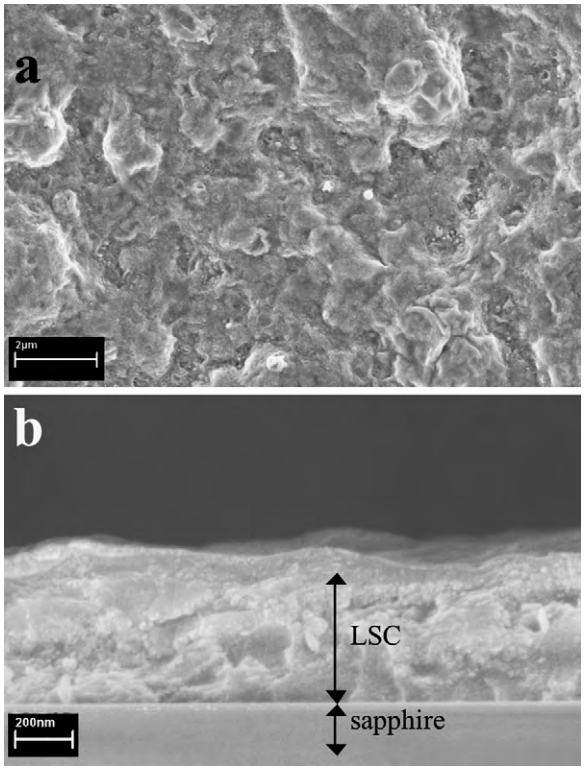

Fig. 1. SEM pictures of an as-deposited LSC thin film prepared by flame for (a) top-view and (b) cross-section spray deposition on a sapphire substrate. The film was deposited within 15 min at 200 °C during flame spray deposition.

The impedance measurements were performed at open circuit voltage (OCV) by applying a sinusoidal voltage of ±10 mV amplitude and measuring the resulting current with a Solartron 1260 frequency response analyzer. The impedance measurements were obtained after heating up the symmetrical cell up to the annealing temperature of the LSC films and then measuring the resistances during the cooling cycle, in steps of 50 °C down to 450 °C. Before acquiring the resistance at every temperature, the samples were left for about 30 min to reach equilibrium. The measurements were performed in a frequency range between 1 MHz and 100 mHz and the recorded impedance spectra were analyzed using the linear least square fit software ZView 2.80 (Scribner Associates, Inc.) with a calculated error sum of squares (χ^2) of less than 10^{-6}.

3. Results and discussion

3.1. Microstructural and structural characterization

Fig. 1, shows the top-view and cross-section images of an as-deposited $La_{0.6}Sr_{0.4}CoO_{3-\delta}$ (LSC) thin film. The film has a thickness of about 450 ± 30 nm and a dense and crack-free microstructure according to the SEM cross-sections. The surface of the film is particle-free, unlike films from other flame-based deposition techniques, such as Combustion Chemical Vapour Deposition (CCVD) and Aerosol Assisted Chemical Vapour Deposition (AACVD) [50].

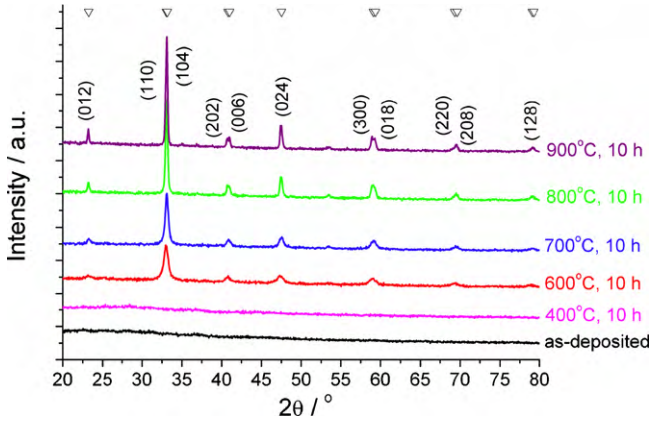

Fig. 2. XRD patterns of a flame spray deposited LSC thin films on sapphire shown as-deposited and after isothermal holds for 10 h for ±3 °C min^{-1}. Reflections of rhombohedral $La_{0.6}Sr_{0.4}CoO_{3-\delta}$ are indicated by (▽), according to JCPDS database reference, PDF Card 01-089-5719.

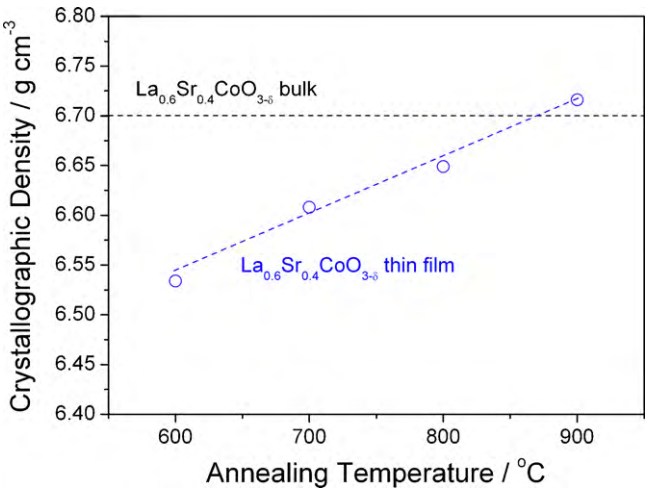

Fig. 3. Crystallographic density of flame-deposited LSC films as a function of annealing temperature for 10 h hold with ±3 °C min^{-1}. Density of bulk $La_{0.6}Sr_{0.4}CoO_{3-\delta}$ according to JCPDS database was added as reference (PDF Card 01-089-5719).

This very high deposition rate of about 30 nm min^{-1} shows the big advantage of the flame spray deposition over other thin film deposition techniques for fast processing of functional crack-free coatings.

A slight thickness variation of ~30 nm can be seen in the topography of the top-view, as well as in the cross-section. Similar observations were made in case of LSCF thin films by spray pyrolysis [52,53]. The authors reported that droplets of a spray pyrolysis process pile up at artificial obstacles or previously deposited droplets on a substrate during a spray deposition process. In the case of the flame spray deposition technique, the deposition mechanism has been investigated by Phase Doppler Anemometry (PDA) measurements and has been confirmed as a droplet deposition [22] similar to the spray pyrolysis. Therefore, the present finding of surface roughness in the order of ~30 nm for the present LSC thin film confirm the droplet deposition character of the flame spray pyrolysis process.

Fig. 2 shows the XRD patterns of as-deposited and 10 h isothermally hold LSC films with respect to temperatures. For film annealing temperatures below 400 °C no distinct XRD reflexes are measurable, and films are amorphous. Increase in temperatures above 400 °C results in occurrence of rhombohedral reflexes and narrowing of the full width of half maxima due to crystallization and the grain growth of the material. Thereby, the amorphous phase transforms directly into the rhombohedral crystal structure during heat treatment (JCPDS database, PDF Card 01-089-5719). Similar direct crystallization from amorphous to crystalline rhombohedral structure was reported in literature [6,9,24,37,54] for various deposition methods, e.g., PLD, metalorganic deposition, spray pyrolysis [6,9,24,55]. The authors reported no dependence on the crystallinity of the YSZ substrate material, e.g., single crystalline versus polycrystalline. In contrast to all these references are the findings of Petrov et al. [56] for bulk LSC with the same composition. According to the phase diagram in [56], the composition of $La_{0.6}Sr_{0.4}CoO_{3-\delta}$ should have a cubic structure above 300 °C. The reason for the rhombohedral composition of the $La_{0.6}Sr_{0.4}CoO_{3-\delta}$ films, instead of the expected cubic, is not clearly understood and it may be due to the oxygen non-stoichiometry in the films, the amount of defects, forming microdomains of perovskite-related phases [56], and/or the amount of organic residues that are still present in the films directly in the amorphous state [57,58].

The annealed LSC films deposited by flame spray deposition show a preferred orientation along (1 1 0)/(1 0 4). This is in accordance with the literature where LSC films deposited by precipitation-based techniques, such as sol–gel [47] and metalorganic deposition [24]. LSC thin films deposited by vacuum-based techniques such as PLD [55] or laser ablation [44] are reported to show substrate-dependent orientation.

Fig. 3 shows the crystallographic density of the LSC thin films as a function of annealing temperature for 10 h isothermal hold. The crystallographic density increases from 6.53 g cm^{-3} at 600 °C to 6.72 g cm^{-3} at 900 °C. Latter density is close to the density of LSC sintered pellets with 6.70 g cm^{-3} of the equal composition (JCPDS database, PDF Card 01-089-5719). In total the crystallographic density increases with annealing temperature by 2.9 relative vol.%. This behaviour can be explained by the increasing ordering of the atoms in the crystal lattice, induced by the thermally activated crystallization. Similar findings have been reported in the literature for precipitation-based ceramic thin films [22,59,60]. A recent study on the crystallization kinetics of ceria thin films deposited by spray pyrolysis by Rupp et al. [61], showed that in precipitation-based metal oxide thin films crystallographic density may even exceed bulk material crystallographic density for fully crystalline films. The choice of organic precursors for film preparation and deposition conditions affect strongly the local near-order of the film at deposition by organic residues acting as space fillers between the metal oxide bond in amorphous state. It was shown that the organic residues strongly affect the history of crystallization and crystallographic density evolvement of the material [57,61].

Fig. 4 shows the SEM top and cross-sectional images of the LSC films annealed isothermally for 4 h at 700 °C, 800 °C, and 900 °C. The films have a porous microstructure that extends throughout the whole thickness of the films independent on annealing temperature. For all films it is observed that the grains grow with increasing annealing temperature, whereas porosity decreases. It is important to note that the surface of the films densifies by annealing, resulting in a gradual decrease of the porosity over the film thickness. Similar findings with large pore size distributions have been reported for LSCF thin films deposited by spray pyrolysis [9]. The authors attributed this to the irregular shape of the pores, with pores that were five times larger than their width [9]. This observation is further supported by the pronounced increase in roughness for high annealing temperatures.

Fig. 5 shows the SEM top-view images of LSC films annealed isothermally at 800 °C or 900 °C with respect to time with heating and cooling rate of 3 °C min^{-1}, respectively.

The porosity in the flame-deposited LSC films decreases with dwell time for all annealing temperatures (Fig. 5). The two major characteristics of the flame-deposited LSC films are: (i) porosity

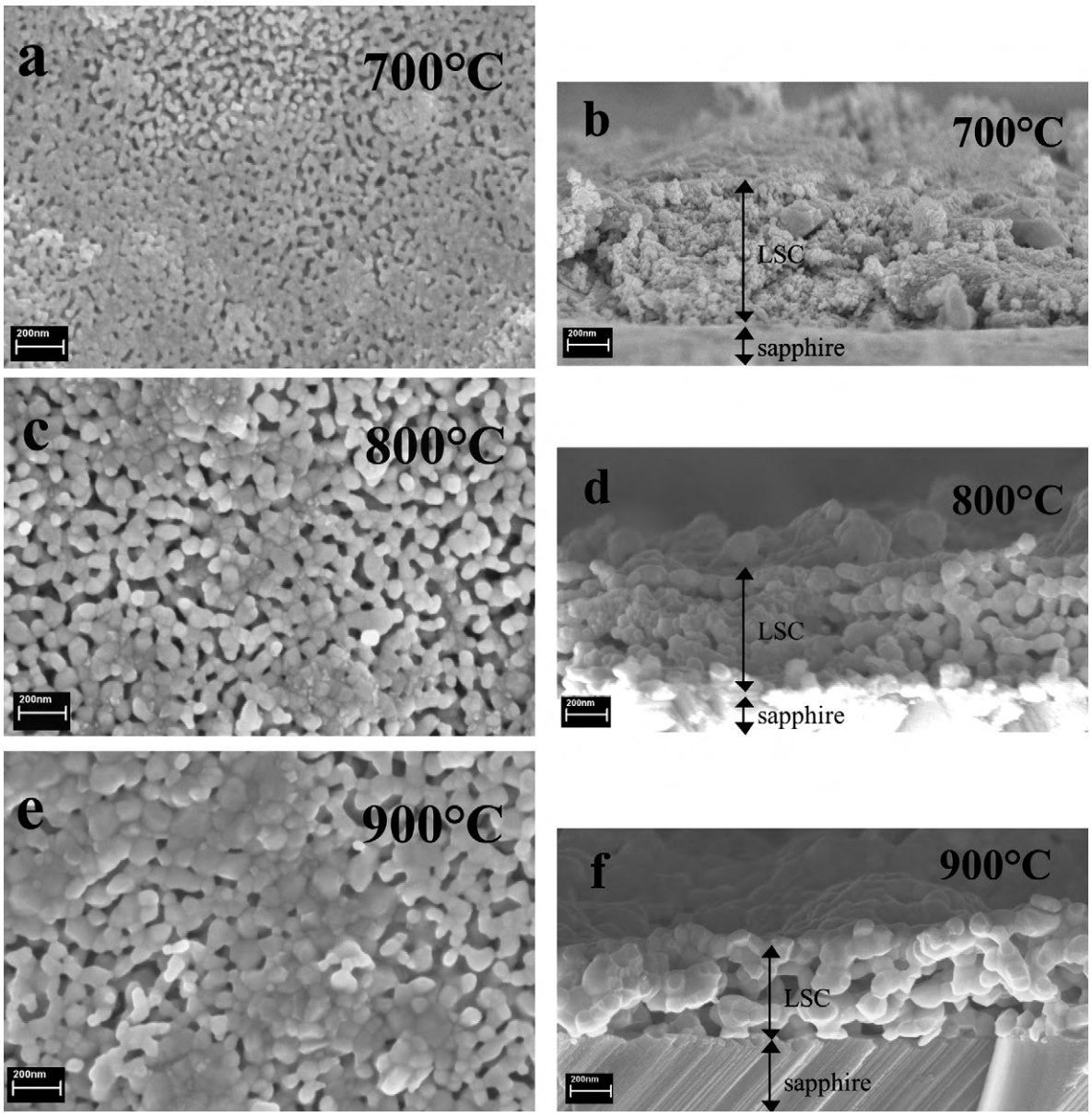

Fig. 4. SEM top-views (a, c, e) and corresponding cross-sections (b, d, f) of flame-deposited LSC thin films. All samples annealed isothermally for 4 h. Heating and cooling rate 3 °C min^{-1}.

forms from an initially dense, amorphous film upon crystallization, and (ii) the porosity decreases with increasing annealing temperature and dwell time. Chen et al. [39] deposited at room temperature LSC thin films on YSZ (1 0 0) single crystals by PLD. The as-deposited films had already a porous microstructure and by annealing from 450 °C to 750 °C porosity increased. Similarly, the as-deposited LSCF PLD films of Beckel et al. [9] were dense and crystalline with a columnar microstructure and developed porosity after annealing above 600 °C. The authors attributed the observed porosity development to solid-state de-wetting. In contrast to these reports is a recent report by Januschewsky et al. [6] on LSC films deposited by PLD, where dense and amorphous LSC films with a columnar structure were deposited at 470 °C on single crystalline YSZ (1 0 0); no porosity developed even after annealing for 22 h at 700 °C. Even for the same material deposited by PLD under very similar conditions [6,39] the trend for the formation of pores by annealing is opposite.

It can be concluded according to the above references that no clear trend with respect to porosity development in LSC-based films during annealing is found to be material specific.

The occurrence of porosity may be related to the different defect levels affecting the LSC or LSCF solid-state de-wetting behaviour and pore formation. Especially in organic-based wet-chemical methods the amount of defect levels is high as organic residues are incorporated between the metal oxide bonds [57]. It is likely that organic precursors are still outgassing in the LSC films processed from the flame technique resulting in pore formation. Interestingly, no pores were observable in case of flame sprayed $Ce_{0.8}Gd_{0.2}O_{1.9-\delta}$ (CGO) thin films for equal organic solvents and use of the salts in nitrate form [22]. Similar observations are reported for the field of spray pyrolysis, where strong porosity was found for LSCF films [9], whereas CGO films [62] remain dense after annealing for equal initial precursor organics. In general, porosity was not observed for $Ce_{0.8}Gd_{0.2}O_{1.9-\delta}$ [22,59,61] and $Y_{0.16}Zr_{0.84}O_{2-\delta}$ thin films [63,64] even though a strong increase in the crystallographic density occurs during annealing and crystallization. A possible reason for the pore formation in the La–Sr-based perovskite films may be the amount of CO_2 that is absorbed by the different nitrate precursors to form carbonates. It is well known that especially Sr forms carbonates

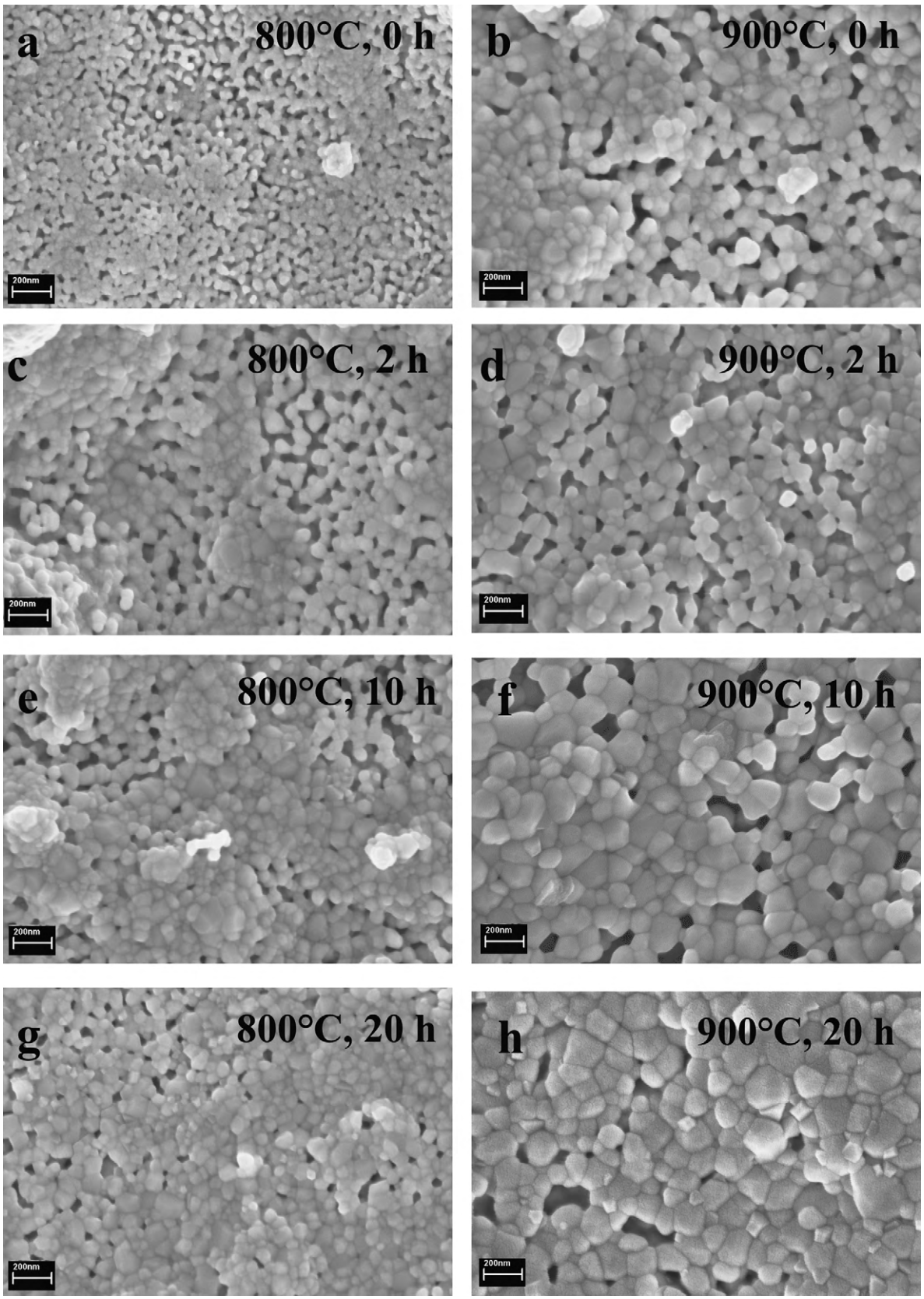

Fig. 5. SEM top-view images of isothermally annealed LSC films as a function of dwell time at 800 °C (a, c, e, g) and 900 °C (b, d, f, h), with heating/cooling rate of 3 °C min^{-1} respectively.

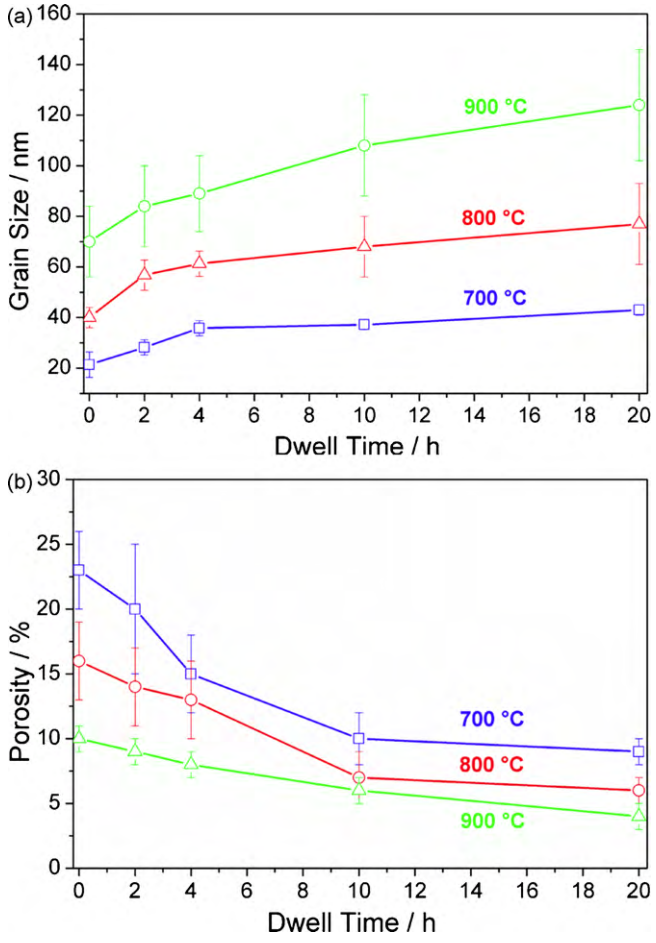

Fig. 6. (a) Average grain size and (b) porosity evolution, respectively of flame spray deposited LSC thin films during isothermal dwells. Error bars, due to calculation error, are also plotted.

easily at rather low temperatures [65–67]. Hence, the formation of pores may be related to the specific salt choice of the precursors of the flame sprayed films for LSC materials.

The results of the grain size deduced from SEM as a function of annealing temperature and isothermal dwell time are presented graphically in Fig. 6(a). Grain growth is a thermally activated process the size of the grains in the LSC films increases as a function of annealing temperature and dwell time. The grains grow for all investigated dwell times and follow parabolic grain growth law in accordance to Burke and Turnbull [68]. The size of the grains in the nanocrystalline LSC films ranges from 21.4 ± 5 nm at 700 °C up to 124 ± 22 nm at 900 °C. Similar parabolic grain growth development with annealing temperature has also been reported for $La_{0.5}Sr_{0.5}CoO_{3-\delta}$ films prepared by sol–gel technique [48] and LSCF films prepared by spray pyrolysis and pulsed laser deposition [9]. Self-limited grain growth as reported in [60,69] was not found possibly due to the porous thin film microstructures. It is known from literature that occurrence of pores strongly affects the grain growth kinetics [70]. Fig. 6(b) summarizes the porosity evolution of the flame-deposited LSC thin films for different annealing temperatures during isothermal dwells of 0–20 h.

3.2. Electrochemical characterization

The flame-deposited LSC films have been characterized electrochemically by impedance spectroscopy in ambient air. The microstructural investigation showed that the post-deposition heat treatment of the films influences the crystal structure, grain size

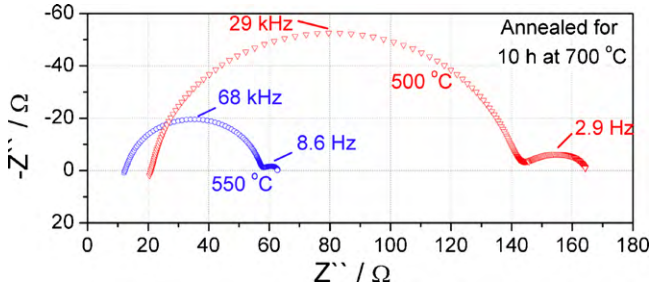

Fig. 7. Typical impedance spectra of a symmetrical cell consisting of a CGO pellet and flame-deposited LSC films measured at 500 °C (▽) and 550 °C (◯). The LSC films were annealed for 10 h at 700 °C prior to electrochemical testing.

and the porosity of the LSC films. Therefore to investigate the influence of the annealing temperature also on the electrochemical performance of the cathode layers, LSC films with a thickness of 200 nm have been deposited symmetrically on a $Ce_{0.9}Gd_{0.1}O_{2-\delta}$ (CGO) pellet and have been annealed isothermally prior to electrochemical testing. Fig. 7 shows two typical Nyquist plots of the impedance spectra obtained from a symmetrical cell with a LSC film annealed for 10 h at 700 °C before testing.

The impedance spectra consist of two arcs, a large one appearing at high frequencies and a smaller one at low frequencies. The data in this study were fitted with the equivalent circuit model shown in Fig. 8. The inductance element L1 accounts for the inductance of the wiring, mainly observed at high frequencies and high temperatures. R1 is assigned to the wire resistances in the measuring device and the two parallel circuits, consisting of a resistance (R2 or R3) and a constant phase element (CPE2 or CPE3) respectively, are attributed to the two observed semi-circles. Various equivalent circuits have been used in the literature to model the impedance spectra of LSC films [42,43,71].

The first semi-circle observed at high frequencies is expected to represent the resistance of the CGO pellet [42] and the one at low frequencies the electrode–electrolyte interface.

The relaxation times, τ, of the two arcs have been calculated according to Eq. (1) and are plotted in an Arrhenius diagram in Fig. 9.

$$\tau = R_x \cdot C_y \quad (1)$$

A linear relationship between the relaxation time of the two semi-circles and the reciprocal temperature is observed. The values of 10^{-5} s up to 10^{-7} s for the relaxation time of the high frequency arc match the reported ones for the CGO pellet [72]. Also, the activation energy of 0.78 eV calculated from an Arrhenius plot of the area specific resistance (ASR) as a function of the reciprocal temperature (not shown here) agrees well with the activation energies between 0.76 eV and 0.85 eV reported in the literature for the CGO grain conduction [72–75]. Even more, the resistance R2 of ~18.1 (obtained from the impedance measurements at 600 °C expressed in conductivity value in view of sample geometry is 0.42 S m, comparable to the conductivity of 0.5 S m at 600 °C reported for the conduction of bulk $Ce_{0.8}Gd_{0.2}O_{1.9}$ pellet [75,76]. Therefore, the high frequency arc is assigned to the contributions of the CGO pellet. Grain boundary conduction at these high temperatures (>450 °C) is not expected to be visualized as a separate arc in the impedance spectra and thus the low frequency arc has to correspond to cathode

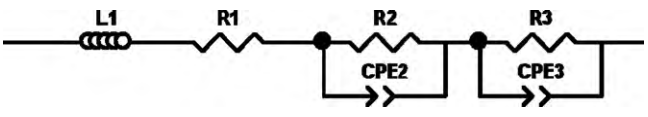

Fig. 8. Equivalent circuit model used for fitting of the measured impedance spectra.

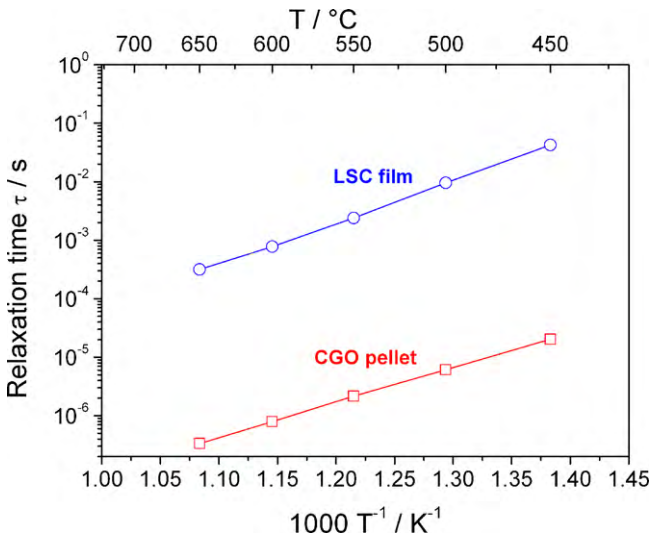

Fig. 9. Relaxation times calculated from the impedance data with Eq. (1) for a symmetrical cell of LSC film/CGO pellet/LSC film, annealed for 10 h at 700 °C.

processes. To confirm this hypothesis, the constant phase elements (CPEs) that were used in the fitting procedure were transformed into chemical capacitances according to Ralph et al. [25]. As a result, the chemical capacitances of the low frequency arc are around 10^{-4} F for the investigated temperatures, which is a typical value for electrode-limited processes [42]. These results, in conjunction with the activation energies of around 1.52 eV described below, show that the low frequency arc can be assigned to the cathode processes.

Fig. 10 shows the area specific resistance (ASR), calculated from the low frequency arc of the impedance spectra as a function of measuring temperature for cells annealed previously for 10 h with respect to temperature.

The cell annealed for 10 h at 400 °C shows the highest resistances. The ASR for this sample is 5.8 Ω cm^2 at 600 °C and has an activation energy of 1.72 eV. The high ASR could be attributed to the amorphous crystal structure of the film as discussed in the microstructural chapter (Fig. 2). Similar results were found in [55] where $La_{0.5}Sr_{0.5}CoO_{3-\delta}$ films prepared by PLD deposited at 450 °C had a very high resistance due to the low crystallinity. The same

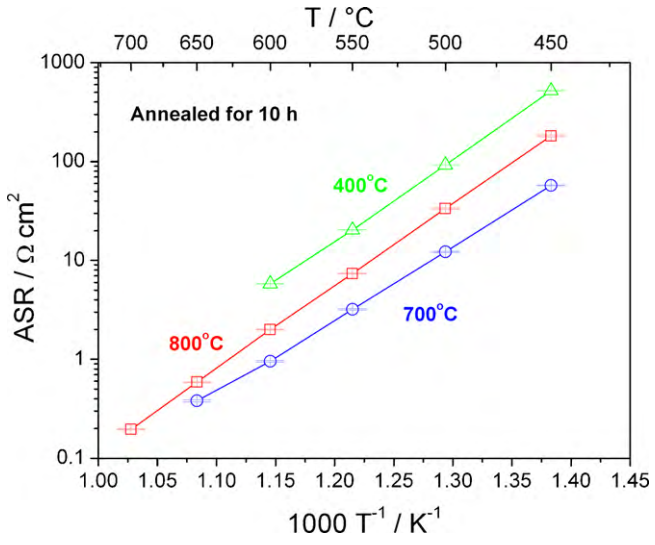

Fig. 10. Area specific resistance (ASR) of LSC symmetrical cells annealed for 10 h at different temperatures, as a function of measuring temperature.

Table 1
ASR values of LSC thin film cathodes prepared by different techniques and measured at 600 °C.

	ASR ((cm^2) at 600 °C	Deposition technique	Reference
$La_{0.6}Sr_{0.4}CoO_{3-\delta}$ (annealed for 10 h at 700 °C)	0.96	Flame spray deposition	this study
$La_{0.5}Sr_{0.5}CoO_{3-\delta}$	0.13	Metalorganic deposition	[24]
$La_{0.6}Sr_{0.4}CoO_{3-\delta}$	0.1	Pulsed laser deposition	[6]

authors reported later a significant enhancement of the oxygen exchange rate in $La_{0.5}Sr_{0.5}CoO_{3-\delta}$ films prepared by PLD for samples annealed at high temperatures (900 °C), due to a roughening of the surface and an increase in the number of electrochemically active surface sites [38]. On the other hand, a recent study on $La_{0.6}Sr_{0.4}CoO_{3-\delta}$ by PLD [6] showed that films with low degree of crystallinity have superior performance (with an ASR of 0.1 Ω cm^2 at 600 °C; low degradation was measured for 24 h for these samples as well). The authors attributed this behaviour mainly to the surface chemistry of the amorphous films, which is supposedly more catalytically active than that of crystalline samples. Therefore, it can be concluded that it is still unclear in the literature, whether the degree of crystallinity, the surface composition or the microstructure is the crucial factor for obtaining high performing LSC cathode films. In this work, the low performance of the LSC films annealed for 10 h at 400 °C is attributed to the amorphous microstructure.

Comparing now the 700 °C and the 800 °C annealed samples it should be noticed that the 800 °C sample has a higher ASR (2 Ω cm^2 at 600 °C) than the 700 °C sample (0.96 Ω cm^2 measured at 600 °C). The activation energies are 1.73 eV and 1.52 eV for 800 °C and 700 °C annealed sample, respectively. In the literature, an activation energy of 1.54 eV for $La_{0.5}Sr_{0.5}CoO_{3-\delta}$ films deposited by sputtering [42] and 1.40 eV for $La_{0.6}Sr_{0.4}CoO_{3-\delta}$ films by PLD [6] was reported. In order to interpret this data, the results from the microstructural characterization are considered. It was found that the sample annealed at 700 °C has smaller grains and higher porosity and have the same rhombohedral structure like the 800 °C. Sase et al. [41] reported that the smaller grains in $La_{0.6}Sr_{0.4}CoO_{3-\delta}$ thin films deposited by PLD resulted in faster oxygen adsorption/desorption rates. Furthermore, it is reported in the literature that for cathodes consisting of mixed electronic-ionic conductors, such as LSC, the rate limiting step in the oxygen reduction mechanism is the oxygen surface exchange [6,21,77,78]. Thus, the higher porosity present in the LSC film annealed at 700 °C is expected to provide more active sites for the oxygen adsorption/desorption exchange, resulting in lower ASR values. In addition, it can be assumed that impurities from the film or the substrate, such as Si, can diffuse better when the annealing temperature is higher and, hence, more negative effect is expected for the 800 °C sample. However, in total the ASR values of the flame-deposited LSC films are one magnitude lower compared to the ones reported for LSC films made by other thin film deposition techniques (Table 1).

In order to satisfy the requirements for cathode in SOFC, the LSC thin films have to be stable in microstructure and electrochemical properties, for long term annealing at elevated temperatures. Therefore, the LSC cells annealed for 10 h at 700 °C and 800 °C, respectively, were measured by impedance spectroscopy for long term, i.e. for 5 days at 550 °C. Data was taken twice per hour. Fig. 11 presents the degradation of these cells in terms of ASR.

The samples annealed at 700 °C have a degradation of 3.9% after 5 days at 550 °C, compared to the degradation of 7% observed for the films annealed at 800 °C (Fig. 11). The enhanced degradation of the samples annealed at 800 °C can be explained by the microstructural characteristics of the films, investigated by XRD and SEM. Fig. 12 shows the XRD patterns of the LSC films before and after

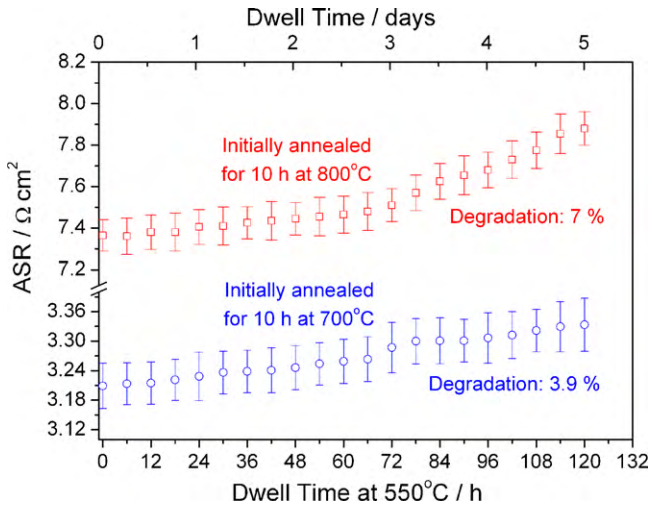

Fig. 11. Degradation of LSC films during an isothermal dwell of 5 days at 550 °C.

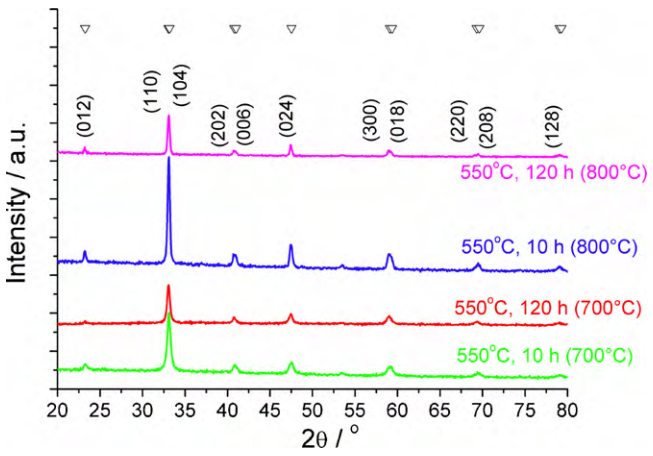

Fig. 12. XRD spectra of LSC thin films before and after impedance measurements at 550 °C, for different initial annealing temperatures indicated in parentheses.

isothermal dwell at 550 °C for 5 days. Both films annealed maintain the perovskite structure even after 5 days at 550 °C. This implies that the LSC films are chemically stable and thus bulk chemical decomposition does not take place.

Fig. 13 shows the microstructural evolution of the LSC films after 5 days at 550 °C, evidenced by SEM top-views. Both films, independent of their initial annealing temperature, have increased grain sizes and less porosity compared to the ones observed for 10 h of annealing. Owing to this increase in the grain size, the number of active sites for oxygen reduction has been drastically reduced, resulting in an increase in the ASR values after the isothermal dwell of 5 days at 550 °C. Compared to the literature, degradation measurements have been performed on $La_{0.5}Sr_{0.5}CoO_{3-\delta}$ films deposited by metalorganic deposition, but only for a short isothermal dwell of 20 h at 850 °C; the ASR appeared to be stable [24]. Furthermore, degradation measurements on $La_{0.6}Sr_{0.4}CoO_{3-\delta}$ powder prepared by the glycine-nitrate combustion method over 5 days [79], showed that in ambient air there is a degradation in the electrochemical performance of about 0.23% per day, owing to surface modification by the formation of strontium hydroxides which inhibit the catalytic sites of the electrode surface. Long term degradation measurements over 5 days have not been reported in the literature for thin films so far.

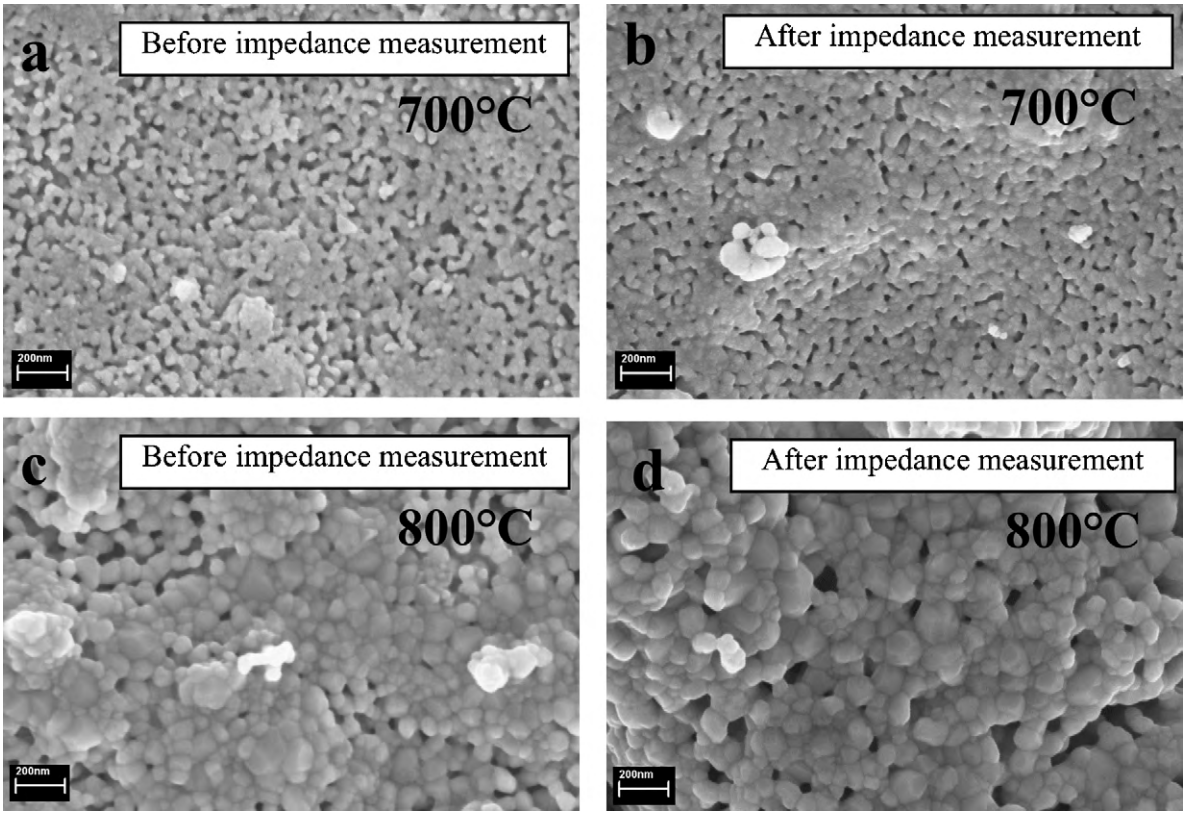

Fig. 13. SEM top-view images of LSC thin films before (a and c) and after impedance measurements (b and d). Impedance measurements were carried out at 550 °C for 120 h: (a) and (b) annealed at 700 °C for 10 h; (c) and (d) annealed at 800 °C for 10 h prior to impedance measurement.

4. Summary and conclusions

$La_{0.6}Sr_{0.4}CoO_{3-\delta}$ (LSC) thin films have been deposited at 200 °C on sapphire substrates and CGO pellets by flame spray deposition. The films have been characterized in terms of microstructure and electrochemical performance. The as-deposited LSC films were dense, particle-free and amorphous, requiring heat treatment for crystallization. By annealing above 600 °C the films develop nanocrystalline grains ranging from 21.4 ± 5 nm at 700 °C up to 124 ± 22 nm at 900 °C. Isothermal grain growth and the development of porosity have been determined as a function of dwell time in order to study the microstructural changes induced during operation. The LSC films develop between 10% and 23% of porosity at the first stages of annealing due to solid-state de-wetting or outgassing of organic residuals and densify with further heat treatment.

Electrochemical measurements performed in ambient air on symmetrical cells showed that crystallinity of the LSC flame sprayed films is required to achieve a reasonable electrochemical performance. LSC films annealed for 10 h at 400 °C were mainly amorphous and thus had high ASR values of 5.8 Ω cm^2 measured at 600 °C with a high activation energy of 1.72 eV. On the other hand, nanocrystalline LSC films annealed at 700 °C showed the lowest ASR value of 0.96 Ω cm^2 measured at 600 °C with a lowered activation energy of 1.52 eV. Higher annealing temperatures than 700 °C increase the ASR again due to grain coarsening, increased density and possibly impurities.

ASR degradation studies performed for 5 days at 550 °C resulted in a degradation of 3.9% for the symmetrical cells annealed at 700 °C and in a degradation of 7% for samples annealed at 800 °C. The results from the microstructural characteristics and the electrochemical performance suggest that flame-deposited LSC cathode films annealed for 10 h at 700 °C may be potential candidates for integration in micro-SOFC applications.

Acknowledgement

Financial support from the Competence Centre for Materials Science and Technology (CCMX) for funding the NANCER project is gratefully acknowledged.

References

[1] S.C. Singhal, Solid State Ionics 135 (2000) 305–313.
[2] S.P.S. Badwal, K. Foger, Ceramics International 22 (1996) 257–265.
[3] J. Will, A. Mitterdorfer, C. Kleinlogel, D. Perednis, L.J. Gauckler, Solid State Ionics 131 (2000) 79–96.
[4] S.B. Adler, Chemical Reviews 104 (2004) 4791–4843.
[5] L.J. Gauckler, D. Beckel, B.E. Buergler, E. Jud, U.P. Muecke, M. Prestat, J.L.M. Rupp, J. Richter, Chimia 58 (2004) 837–850.
[6] J. Januschewsky, M. Ahrens, A. Opitz, F. Kubel, J. Fleig, Advanced Functional Materials 19 (2009) 1–6.
[7] F. Zhao, R. Peng, C. Xia, Materials Research Bulletin 43 (2008) 370–376.
[8] A. Heel, P. Holtappels, P. Hug, T. Graule, Fuel Cells 10 (2010) 419–432.
[9] D. Beckel, A. Dubach, A.N. Grundy, A. Infortuna, L.J. Gauckler, Journal of the European Ceramic Society 28 (2008) 49–60.
[10] J. Shao, S.M. Haile, Nature 431 (2004) 170–173.
[11] J. Pena-Martinez, D. Marrero-Lopez, J.C. Ruiz-Morales, B.E. Buergler, P. Nunez, L.J. Gauckler, Journal of Power Sources 159 (2006) 914–921.
[12] Z. Yang, A.S. Harvey, L.J. Gauckler, Scripta Materialia 61 (2009) 1083–1086.
[13] Z. Yang, A.S. Harvey, A. Infortuna, L.J. Gauckler, Journal of Applied Crystallography 42 (2009) 153–160.
[14] A.S. Harvey, F.J. Litterst, Z. Yang, J.L.M. Rupp, A. Infortuna, L.J. Gauckler, Physical Chemistry Chemical Physics 11 (2009) 3090–3098.
[15] M. Arnold, T.M. Gesing, J. Martynczuk, A. Feldhoff, Chemistry of Materials 20 (2008) 5851–5858.
[16] A. Feldhoff, J. Martynczuk, M. Arnold, M. Myndyk, I. Bergmann, V. Sepelak, W. Gruner, U. Vogt, A. Hahnel, J. Woltersdorf, Journal of Solid State Chemistry 182 (2009) 2961–2971.
[17] A. Mitterdorfer, L.J. Gauckler, Solid State Ionics 111 (1998) 185–218.
[18] S.P. Simner, J.P. Shelton, M.D. Anderson, J.W. Stevenson, Solid State Ionics 161 (2003) 11–18.
[19] Y.L. Liu, A. Hagen, R. Barfod, M. Chen, H.J. Wang, F.W. Poulsen, P.V. Hendriksen, Solid State Ionics 180 (2009) 1298–1304.
[20] M. Matsuda, K. Ihara, M. Miyake, Solid State Ionics 172 (2004) 57–61.
[21] E.V. Tsipis, V.V. Kharton, Journal of Solid State Electrochemistry 12 (2008) 1367–1391.
[22] N.I. Karageorgakis, A. Heel, T. Graule, L.J. Gauckler, Solid State Ionics, submitted for publication, SSI-D-09-00533.
[23] A. Stoermer, J.L.M. Rupp, L.J. Gauckler, Solid State Ionics 177 (2006) 2075–2079.
[24] C. Peters, A. Weber, E. Ivers-Tiffee, Journal of the Electrochemical Society 155 (2008) 730–737.
[25] J.M. Ralph, A.C. Schoeler, M. Krumpelt, Journal of Materials Science 36 (2001) 1161–1172.
[26] J.P.P. Huijsmans, F.P.F.v. Berkel, G.M. Christie, Journal of Power Sources 71 (1998) 107–110.
[27] A. Evans, A. Bieberle-Hutter, J.L.M. Rupp, L.J. Gauckler, Journal of Power Sources 194 (2009) 119–129.
[28] A. Bieberle-Hutter, D. Beckel, A. Infortuna, U.P. Muecke, J.L.M. Rupp, L.J. Gauckler, S. Rey-Mermet, P. Muralt, N.R. Bieri, N. Hotz, M.J. Stutz, D. Poulikakos, P. Heeb, P. Muller, A. Bernard, R. Gmur, T. Hocker, Journal of Power Sources 177 (2008) 123–130.
[29] D. Beckel, A. Bieberle-Hutter, A. Harvey, A. Infortuna, U.P. Muecke, M. Prestat, J.L.M. Rupp, L.J. Gauckler, Journal of Power Sources 173 (2007) 325–345.
[30] H. Huang, M. Nakamura, P.C. Su, R. Fasching, Y. Saito, F.B. Prinz, Journal of the Electrochemical Society 154 (2007) 20–24.
[31] J.H. Shim, C.-C. Chao, H. Huang, F.B. Prinz, Chemistry of Materials 19 (2007) 3850–3854.
[32] A.C. Johnson, A. Baclig, D.V. Harburg, B. Lai, S. Ramanathan, Journal of Power Sources 195 (2010) 1149–1155.
[33] P. Su, C. Chao, J.H. Shim, R. Fasching, F.B. Prinz, Nano Letters 8 (2008) 2289–2292.
[34] U.P. Muecke, D. Beckel, A. Bernard, A. Bieberle-Hutter, S. Graf, A. Infortuna, P. Muller, J.L.M. Rupp, J. Schneider, L.J. Gauckler, Advanced Functional Materials 18 (2008) 3158–3168.
[35] J.L.M. Rupp, U.P. Muecke, P.C. Nalam, L.J. Gauckler, Journal of Power Sources 195 (2010) 2669–2676.
[36] A.C. Johnson, B.-K. Lai, H. Xiong, S. Ramanathan, Journal of Power Sources 186 (2009) 252–260.
[37] E. Koep, C. Jin, M. Haluska, R. Das, R. Narayan, K. Sandhage, R. Snyder, M. Liu, Journal of Power Sources 161 (2006) 250–255.
[38] X. Chen, S. Wang, Y.L. Yang, L. Smith, N.J. Wu, B.-I. Kim, S.S. Perry, A.J. Jacobson, A. Ignatiev, Solid State Ionics 146 (2002) 405–413.
[39] X. Chen, N.J. Wu, D.L. Ritums, A. Ignatiev, Thin Solid Films 342 (1999) 61–66.
[40] D. Mori, H. Oka, Y. Suzuki, N. Sonoyama, A. Yamada, R. Kanno, Y. Sumiya, N. Imanishi, Y. Takeda, Solid State Ionics 177 (2006) 535–540.
[41] M. Sase, J. Suzuki, K. Yashiro, T. Otake, A. Kaimai, T. Kawada, J. Mizusaki, H. Yugami, Solid State Ionics 177 (2006) 1961–1964.
[42] A. Bieberle-Hutter, M. Sogaard, H.L. Tuller, Solid State Ionics 177 (2006) 1969–1975.
[43] N. Imanishi, T. Matsumura, Y. Sumiya, K. Yoshimura, A. Hirano, Y. Takeda, D. Mori, R. Kanno, Solid State Ionics 174 (2004) 245–252.
[44] D. Waller, L.G. Coccia, J.A. Kilner, I.W. Boyd, Solid State Ionics 134 (2000) 119–125.
[45] A. Endo, H. Fukunaga, C. Wen, K. Yamada, Solid State Ionics 135 (2000) 353–358.
[46] J.V. Mantese, A.L. Micheli, A.B. Catalan, N.W. Schubring, Applied Physics Letters 64 (1994) 3509–3511.
[47] R. Chiba, F. Yoshimura, Y. Sakurai, Y. Tabata, M. Arakawa, Solid State Ionics 175 (2004) 23–27.
[48] L. Dieterle, D. Bach, R. Schneider, H. Stormer, D. Gerthsen, U. Guntow, E. Ivers-Tiffee, A. Weber, C. Peters, H. Yokokawa, Journal of Materials Science 43 (2008) 3135–3143.
[49] K.-J. Lee, J.-W. Park, J.-K. Yang, K.-S. Lee, Y.-H. Choa, Materials Science and Engineering A 449–451 (2007) 774–777.
[50] K.L. Choy, Progress in Materials Science 48 (2003) 57–170.
[51] S.L.d.S.e. Lucato, Lince Softwarein, Department of Material Science, Darmstadt University of Technology, Darmstadt, Germany, 1999.
[52] D. Beckel, D. Briand, A.R. Studart, N.F.d. Rooij, L.J. Gauckler, Advanced Materials 18 (2006) 3015–3018.
[53] D. Beckel, D. Briand, A. Bieberle-Hutter, J. Courbat, N.F.d. Rooij, L.J. Gauckler, Journal of Power Sources 166 (2007) 143–148.
[54] Y.L. Yang, C.L. Chen, S.Y. Chen, C.W. Chu, A.J. Jacobson, Journal of The Electrochemical Society 147 (2000) 4001–4007.
[55] X. Chen, N. Wu, A. Ignatiev, Z. Zhang, W.-K. Chu, Thin Solid Films 350 (1999) 130–137.
[56] A.N. Petrov, O.F. Kononchuk, A.V. Andreev, V.A. Cherepanov, P. Kofstad, Solid State Ionics 80 (1995) 189–199.
[57] J.L.M. Rupp, B. Scherrer, L.J. Gauckler, Physical Chemistry Chemical Physics, submitted for publication.
[58] J. Malek, S. Matsuda, A. Watanabe, T. Ikegami, T. Mitsuhashi, Thermochimica Acta 267 (1995) 181–194.
[59] J.L.M. Rupp, C. Solenthaler, P. Gasser, U.P. Muecke, L.J. Gauckler, Acta Materialia 55 (2007) 3505–3512.
[60] J.L.M. Rupp, A. Infortuna, L.J. Gauckler, Acta Materialia 54 (2006) 1721–1730.
[61] J.L.M. Rupp, B. Scherrer, A.S. Harvey, L.J. Gauckler, Advanced Functional Materials 19 (2009) 1–10.
[62] J.L.M. Rupp, L.J. Gauckler, Solid State Ionics 177 (2006) 2513–2518.
[63] S. Heiroth, T. Lippert, A. Wokaun, M. Dobeli, Applied Physics A 93 (2008) 639–643.
[64] S. Heiroth, T. Lippert, A. Wokaun, M. Dobeli, J.L.M. Rupp, B. Scherrer, L.J. Gauckler, Journal of the European Ceramic Society 30 (2010) 489–495.

[65] G. Juhasz, Z. Homonnay, K. Nomura, T. Hayakawa, S. Hamakawa, A. Vertes, Solid State Ionics 139 (2001) 219–231.
[66] Z. Homonnay, K. Nomura, G. Juhasz, E. Kuzmann, S. Hamakawa, T. Hayakawa, A. Vertes, Journal of Radioanalytical and Nuclear Chemistry 255 (2003) 425–429.
[67] K. Nomura, K. Tokumistu, T. Hayakawa, Z. Homonnay, Journal of Radioanalytical and Nuclear Chemistry 246 (2000) 69–77.
[68] J.E. Burke, D. Turnbull, Progress in Metal Physics 3 (1952) 220–292.
[69] N.I. Karageorgakis, A. Heel, J.L.M. Rupp, M.H. Aguirre, T. Graule, L.J. Gauckler, Advanced Functional Materials, submitted for publication.
[70] M.N. Rahaman, Y.C. Zhou, Journal of the European Ceramic Society 15 (1995) 939–950.
[71] H. Schichlein, A.C. Muller, M. Voigts, A. Krugel, E. Ivers-Tiffee, Journal of Applied Electrochemistry 32 (2002) 875–882.
[72] A. Jasper, J.A. Kilner, D.W. McComb, Solid State Ionics 179 (2008) 904–908.
[73] H. Inaba, H. Tagawa, Solid State Ionics 83 (1996) 1–16.
[74] C. Kleinlogel, L.J. Gauckler, Solid State Ionics 135 (2000) 567–573.
[75] M. Mogensen, N.M. Sammes, G.A. Tompsett, Solid State Ionics 129 (2000) 63–94.
[76] K. Eguchi, T. Setoguchi, T. Inoue, H. Arai, Solid State Ionics 52 (1992) 165–172.
[77] A. Ringuede, J. Fouletier, Solid State Ionics 139 (2001) 167–177.
[78] S.B. Adler, X.Y. Chen, J.R. Wilson, Journal of Catalysis 245 (2007) 91–109.
[79] P. Hjalmarsson, M. Sogaard, M. Mogensen, Solid State Ionics 179 (2008) 1422–1426.